From the van der Waals dimer to the solid state of mercury with relativistic *ab initio* and density functional theory

Nicola Gaston and Peter Schwerdtfeger
Center of Theoretical Chemistry and Physics, Institute of Fundamental Sciences, Massey University (Albany Campus), Private Bag 102904, North Shore MSC, Auckland, New Zealand
(Received 12 March 2006; published 14 July 2006)

A comprehensive study of small mercury clusters is presented using relativistic coupled cluster, many-body perturbation, and density functional theory starting from the dimer potential, to small clusters and to the solid state. In all these calculations we employ an energy-consistent small core relativistic pseudopotential. We address the possibilities for the simulation of larger clusters. Both Lennard-Jones and alternative isomers are considered as candidate structures for the global minimum, and both isotropic and anisotropic polarizabilities are determined for $N \leq 24$. We address the well-known nonconvergence of the many-body expansion of the interaction potential. We show that a two-body potential cannot describe the rhombohedral distortion from a face centered cubic structure. Density functional theory seems to have similar difficulties with the exception of the local density approximation. We therefore suggest a two-body correlation potential to be used to correct the Hartree-Fock energy, which already contains the important many-body effects. Within this approach we obtain good agreement with the best-known reference data ranging from the dimer to the solid state.

DOI: 10.1103/PhysRevB.74.024105 PACS number(s): 71.15.−m, 71.15.Mb, 31.25.−v, 34.20.Cf

I. INTRODUCTION

Clusters are interestingly situated between two extreme systems; to one side lie small molecules such as the dimer, and at the other is the very different system of an infinite periodic lattice. This vision of connecting the two limits upon varying the number of atoms (N) is at the heart of cluster physics due to the marked way in which properties of clusters vary with size. The possibility of tuning, for example, electric and optical responses of clusters as a function of size implies a wide range of applications. This is indicated by the large number of cluster systems that have been studied so far.[1–4]

Mercury clusters are of particular interest as the contrast between the dimer and bulk is most marked; the dimer and small clusters are van der Waals-like (and therefore comparable to the noble gas clusters) whereas the bulk is metallic. This is exemplified by a rather large change in the bonding distance, from 3.7 Å for the dimer[5] to 3.0 Å for the solid.[6] An early paper found deviations from van der Waals behavior already at a size of about 12 atoms, and noted behavior at $N=13$ that defied the trend, marking it as a uniquely symmetric icosahedral structure.[7] This is consistent with arranging close-packed spheres on the surface of a sphere, and found typically in Lennard-Jones clusters[8] which maximize the number of bonding interactions. In 1992 Rademann, Hensel, and co-workers published a study of the photoelectron spectra of the neutral clusters of sizes up to 200 atoms.[9] They observed a non-structured absorption between 4.3 and 6.3 eV up to a cluster size of 13 atoms, but found that for clusters of 20 or more atoms the observed spectra fit closely the Drude model of metallic mercury, and they extracted approximate bond lengths of 3.1 Å, known to be much closer to the bulk value than that of the dimer. This was accompanied by a similar work of Kaiser and Rademann,[10] who found that cluster sizes of about 60 atoms were sufficient for there to be a high density of p states near the Fermi level. Moreover, theoretical (tight-binding linear muffin-tin) calculations available at the time[11] found an increase of $6p$ character in clusters between 13 and 19 atoms, indicating an increase in covalency. The $6p$ character of a cluster of 79 atoms was also found to agree very closely with the bulk value.[11,12] A study of caesium-mercury clusters (Hg_NCs^+) also agreed with the assumption of a transition from van der Waals to covalent bonding at a relatively small size of about 30 atoms.[13]

Later experiments would disagree strongly with these first findings. In contrast to the prediction by Singh and Dy of the onset of metallicity at around $N=80$,[11] a study of the $6s$-$6p$ gaps of negatively charged mercury clusters in 1998 by Cheshnovsky and co-workers predicted a much higher value for the onset of metallicity, at an extrapolated value of 400 atoms. Their data covered the range $3 \leq N \leq 250$.[14] At this stage it became clear that the simple concept of a metal to nonmetal transition at small sizes, which has been very useful in much of cluster physics, must become in the case of mercury a very complicated evolution from van der Waals behavior at small sizes, gradually to covalently bound clusters, and then eventually to the metallic state. However, this is no simple monotonic behavior, as it is constantly interrupted by the changing structure of the clusters themselves. For small clusters the addition of a single atom may change many properties significantly though the underlying structural motif is constant, such as is observed with the completion of the icosahedron on going from 12 atoms to 13. In large clusters the impact of adding a single atom may be apparently less, except that at particular sizes competing geometries which have different "magic numbers" may lead again to highly size-dependent characteristics.

The current challenge for computational physics is to approach the much larger sizes at which the nonmetal to metal transition for mercury has been predicted experimentally. This is no trivial task as the methods that have been proven accurate for small sizes are expensive in computer time, re-

quiring a high-level treatment of electron correlation and relativistic effects together with large basis sets to suppress the basis set superposition error. Previous theoretical studies have been restricted to large-core pseudopotentials for the calculation of clusters only up to $N=15$,[15–18] and more recently up to $N=14$ by Hartke and co-workers.[19,20] For larger cluster sizes towards the metallic state single-reference electron correlation procedures will fail and a multireference treatment becomes impossible. On the other hand, methods that have been used for the optimization of noble gas clusters (e.g., a Lennard-Jones or effective two-body potential fitted to the dimer curve) have been shown to be problematic for mercury, due to the poor convergence of the many-body expansion which requires at the very least the inclusion of three- and four-body forces.[22] This poor convergence is usually attributed to the non-metal to metal transition and consequent bond shortening which implies that at shorter distances than the dimer bond length, a two-body potential is not sufficient anymore.[25] In contrast, for the noble gases the dimer and solid bond distances are very close and this problem does not occur, although at shorter distances (accessible under high pressure) many-body effects will eventually become important.[26] It remains to be seen if, for example, correlation effects can be parametrized using a simple two-body potential, as a way of improving on the poor convergence of the many-body series for the total energy of mercury clusters as has been previously mentioned.[22–24] Finally, density functionals are currently not accurate enough to describe interactions between mercury atoms from the dimer to the solid state.

In this work we would like to establish the global minimum structures of small mercury clusters as they have been claimed recently to deviate substantially from known Lennard-Jones systems.[19,20] We therefore considered the static dipole polarizabilities of these clusters as they are usually sensitive to the particular cluster structure. They also provide a possible indicator of van der Waals or covalent character, as has been seen, for example, for zinc.[27] Experimentally, static electric dipole polarizabilities of metal clusters may be measured by electric field deflection of a molecular beam. Such results already exist for sodium,[28] nickel,[29] niobium,[30] and copper[31] clusters, for example. In the case of sodium, a correlation is seen between the electronic shell structure and the polarizability, as can be understood for a jellium-type metal; on the other hand for niobium a very large variation in polarizability (a factor of 7 over a change of three atoms in size) is observed which must be due to large variations in geometrical structure. In the case of mercury we expect the second result to be most applicable. We then extend our cluster studies to the solid state and present optimized lattice parameters and cohesive energies for bulk mercury.

II. METHODS

The Hg dimer is a well known example of a van der Waals molecule, for which a good description of correlation is essential and density functional theory (DFT) could be deficient. Thus as the first step in our study of mercury clusters we have examined the dimer binding potential. The Zn, Cd, and Ba dimers are also included for comparison. The calculations have been performed using both the GAUSSIAN03 and MOLPRO codes.[32,33] The basis sets used to assess the performance of the different methods was chosen to be as large as practical to suppress the basis set superposition error (BSSE). For this we chose correlation consistent basis sets obtained by minimizing the atomic energy at the second-order many-body (Møller-Plesset) perturbation level of theory, abbreviated as MBPT2 in the following. For Hg, Cd, Zn, and Ba, these large Gaussian basis sets consist of uncontracted $(11s10p9d4f)$ functions with the core described by small core Stuttgart pseudopotentials.[34] Various density functionals have been employed as well as Hartree-Fock (HF), MBPT2, and coupled cluster procedures [CCSD(T)] for comparison. All calculations were performed with a full active orbital space, i.e., 20 electrons per atom to be correlated over the full virtual space.

Based on the performance observed for the Hg dimer, the PW91 functional was further chosen for the cluster optimizations, along with MBPT2 and CCSD(T) (up to $N=9$ and $N=7$, respectively). The local density approximation (LDA) functional was used for comparison as it describes the solid structure most accurately. As starting points in our geometry optimizations, we have chosen the Lennard-Jones type structures obtained from simulated annealing calculations using two- and effective three-body potentials as described in detail by Moyano *et al.*,[22] starting from geometries found at the Cambridge Cluster Database,[8] as well as the recently published alternative structures by Hartke and co-workers.[19] Here we used smaller correlation consistent basis sets for mercury, i.e., a contracted $(6s5p4d1f)$ to $[4s4p3d1f]$ set (denoted as small in the following). The accuracy of this basis set was assessed using the counterpoise procedure for the BSSE of Boys and Bernardi.[35]

We have also considered the problem of determining the structures of large mercury clusters. The nonconvergence of the many-body expansion in mercury requires not only three-body but also higher many-body effects to be included.[22] However, it has been shown that the correlation energy for Hg_2 is largely a two-body effect,[25] and therefore a two-body correlation potential has been obtained by taking the difference between the best known dimer curve (of Ref. 36) and the Hartree-Fock curve calculated with a rather large uncontracted basis set including g and h functions $(11s10p9d4f3g2h)$. The resulting two-body correlation curve was used as a correction to HF. This has the advantage that the BSSE at the HF level of theory is relatively small compared to correlated calculations. The applicability of this approach ranges from the dimer to the solid state. The program used for the solid-state calculations of mercury was CRYSTAL.[37] A small contracted basis set which was optimized for HF calculations has been used for the solid-state calculations.[38]

The small correlation consistent basis set used for the coupled cluster calculations was further improved for polarizability calculations by the addition of diffuse s and p functions, and an extra f function. The size of this basis set, coupled with its good performance for the atomic polarizability means that these calculations can be extended to rea-

sonably large cluster sizes. Following the definitions of Buckingham,[39] we can write the energy of an uncharged molecule in a weak, static, homogeneous electric field as

$$E^p = E^0 - \mu_\alpha F_\alpha - \frac{1}{2}\alpha_{\alpha\beta}F_\alpha F_\beta + \cdots, \quad (1)$$

where E^0 is the energy of the free molecule, μ_α is the dipole moment, F_α, etc., is the electric field, and $\alpha_{\alpha\beta}$ is the static dipole polarizability. Here we use the Einstein sum convention. The subscripts denote Cartesian coordinates x, y, z. The number of independent components of the polarizability tensor is symmetry dependent, and thus we define an isotropic polarizability dependent on the cluster size N,

$$\alpha(N) = \mathrm{tr}[\alpha_{\alpha\beta}(N)]/3 \quad (2)$$

which is orientation independent and accessible by experiment. The polarizability anisotropy is calculated from the polarizability tensor [denoted as $(\alpha_{\alpha\beta})$] as

$$\begin{aligned}\beta(N) &= +\left(\frac{1}{2}(3\ \mathrm{tr}\{[\alpha_{\alpha\beta}(N)]^2\} - \{\mathrm{tr}[\alpha_{\alpha\beta}(N)]\}^2)\right)^{1/2} \\ &\overset{\alpha\ \mathrm{diag}}{=} +\left(\frac{1}{2}\{[\alpha_{11}(N) - \alpha_{22}(N)]^2 + [\alpha_{11}(N) - \alpha_{33}(N)]^2 \right. \\ &\quad \left. + [\alpha_{22}(N) - \alpha_{33}(N)]^2\}\right)^{1/2}. \quad (3)\end{aligned}$$

The polarizability tensor has been calculated analytically using the PW91 functional as implemented in GAUSSIAN03, as this gives very good results for the mercury atom.[32] The choice of basis set is particularly sensitive for polarizability calculations, but in order to extend these calculations to larger cluster sizes, the size of the basis set had to be kept relatively small. We therefore improved our small correlation consistent basis set optimized for the CCSD(T) calculations for the polarizability calculations by the addition of diffuse s and p functions, and an extra f function. This basis set is therefore referred to as the small+spf basis set.

III. RESULTS AND DISCUSSION

A. Dimers

The Hg dimer is more strongly bound than the Zn and Cd dimers due to relativistic effects and to a lesser extent the lanthanide contraction, which shorten the Hg_2 bond substantially.[40,41] Although barium is not a transition metal, it is a metal with a closed $6s$ valence shell and similar in size compared to mercury. Moreover, barium is also influenced by relativistic effects which makes a comparison interesting. Studies of Ba_N cluster structures have shown similar results to those of mercury and of the noble gases.[42] The currently most accurate Hg_2 CCSD(T) potential curve calculated with the same large basis set includes spin-orbit effects[36] is shown in Fig. 1 together with the HF and DFT curves. The HF curve is included as to give an idea of the effect of electron correlation in binding the dimer. It is not surprising that HF fails to describe van der Waals bonding, which may be considered to be entirely due to electron correlation, but the functionals B3LYP and BPW91 fail almost as badly, with BP86 showing just a slight improvement. LDA is typically overbinding, by about a factor of 3. It is therefore evident that DFT gives widely varying results for Hg_2, depending on the functional chosen. It is however the PW91 functional (PW91 for both exchange and correlation) that gives by far the most realistic curve. It produces a curve which has a slightly shorter equilibrium bond length than either MBPT2 or CCSD(T), but a binding energy intermediate between the two, and at long range (above 4 Å) matches the CCSD(T) curve closely. However, all functionals show the wrong behavior at long range, as they do not correctly describe Van der Waals interactions. A summary of the performance of these methods for Hg_2 (bond lengths, dissociation energies, and vibrational frequencies) is given in Table I, along with the results for Zn, Cd, and Ba.

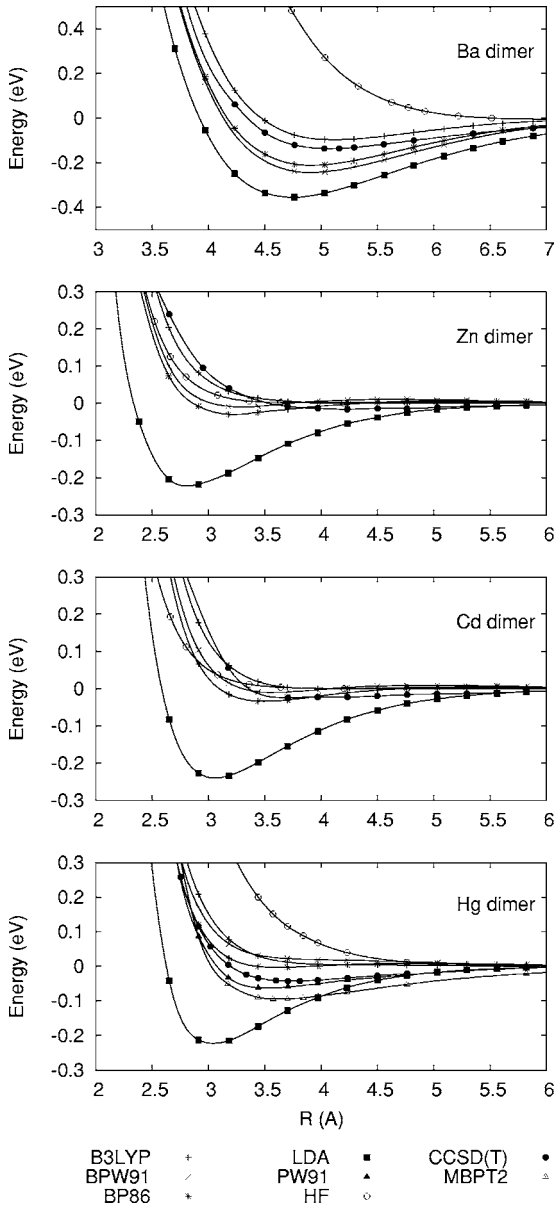

FIG. 1. DFT, HF, and CCSD(T) potential curves for the Hg, Cd, Zn, and Ba dimers.

TABLE I. Spectroscopic parameters for the Hg, Cd, Zn, and Ba dimers. Dissociation energies are in eV, bond lengths in Å, and frequencies in cm^{-1}. The experimental data for Cd_2 and Zn_2 are from Ref. 43, for Hg_2, from Ref. 44, and for Ba_2 only theoretical reference data are available (Ref. 45).

	Bond length at potential minimum r_e			
Method	Hg_2	Cd_2	Zn_2	Ba_2
B3LYP				5.124
BP86		3.499	3.213	4.910
BPW91		3.567	3.302	4.902
PW91	3.522	3.441	3.173	4.360
Xα	3.128	3.158	2.930	4.925
LDA	3.040	3.055	2.810	4.749
CCSD(T)	3.772	3.738	4.215	5.079
Expt	3.69	4.07	4.19	4.881
	Dissociation energy at potential minimum D_e			
Method	Hg_2	Cd_2	Zn_2	Ba_2
B3LYP				0.0968
BP86		0.0308	0.0432	0.2126
BPW91		0.0008	0.0246	0.2436
PW91	0.0614	0.0867	0.0829	0.4152
Xα	0.1591	0.1876	0.1457	0.2473
LDA	0.2206	0.2698	0.2116	0.3549
CCSD(T)	0.0443	0.0359	0.0380	0.1368
Expt	0.0471	0.0410	0.0346	0.2020
	Harmonic vibrational frequency ω_e			
Method	Hg_2	Cd_2	Zn_2	Ba_2
B3LYP			65.7	9.8
BP86		33.6	53.1	41.3
BPW91			40.4	42.9
PW91	25.7	35.5	49.8	23.4
Xα	46.3	54.6	65.7	40.1
LDA	55.0	70.4	88.5	47.5
CCSD(T)	21.5	23.1	27.4	32.8
Expt	19.7	23.0	25.9	35.0

The various potential curves for Cd_2 are given for a range of density functionals, as well as the CCSD(T) and HF results. The picture for Cd is very similar to that for Hg, although the generalized gradient approximation (GGA) functionals behave on the whole a little better. Of the functionals tested, only B3LYP is entirely repulsive. Again for Zn the overall picture is much the same. It is, however, noticeable that the difference in bond length between DFT and CCSD(T) is largest for Zn_2, close to 1 Å apart. However, while DFT consistently predicts the Zn dimer bond length to be shorter than Cd, the experimental values are 4.07 Å for Cd, and 4.19 Å for Zn. This compares reasonably well with the CCSD(T) values given here 3.738 and 4.215 Å, respectively.

The potential curves for Ba_2 are also shown in Fig. 1. The overall behavior of all methods for Ba is considerably better than for Hg. In particular, the GGA-corrected functionals are all binding, and the agreement between DFT and CCSD(T) is in general much better. This demonstrates the polarization of the underlying *d* core for the group 12 transition metals, especially for Hg where the 5*d* electrons are relativistically destabilized. Hence the failure of DFT to correctly describe the van der Waals bonding at long range, where considerable overlap takes place and polarization of the *d* core becomes important.

B. Hg_N clusters

It is well known that up to some cluster size the noble gases adopt highly symmetric icosahedral structures that are obtained using a simple Lennard-Jones (LJ) type model (for a detailed discussion see Ref. 21). LJ type clusters maximize the number of interactions between the atoms. Therefore the structures are as close to spherical as can be managed to minimize surface effects. These result from the essentially isotropic van der Waals forces and the lack of overlap effects, and so have commonly been assumed to apply to mercury clusters as well. Of course, as the nature of the Hg-Hg bond changes from van der Waals to covalent with increasing cluster size *N*, the existence of non-LJ isomers becomes more likely. However, simulated annealing results of Moyano *et al.*[22] using two- and three-body potentials constructed from relativistic coupled cluster and second-order many-body perturbation theory show behavior in agreement with the LJ potential, and have the familiar "magic numbers" at $N=6$, 13, 19, 23, 26, and 29 atoms. In contrast, in a recent paper Hartke *et al.* proposed several novel low-symmetry structures as the global minima for Hg clusters.[19] These appeared curiously disordered when compared to more commonly known LJ or Morse type structures, and a vibrational analysis was performed in order to test their stability. The model used was that of an effective dispersion potential based on accurate calculations of the dimer, and added to the HF energy to include correlation effects.[46] The structures proposed by Hartke *et al.* covered the size range of 7 to 14 atoms and show a tendency towards tetrahedron-based structures.

The optimized structures at the *ab initio* and DFT level of theory are summarized in Table II. The results for the optimized Hartke clusters are given in Table III. The corresponding minimum energy structures are pictured in Fig. 2 and labeled as isomers 7b through 14b. The MBPT2 clusters should be considerably more reliable than the DFT results; however, even MBPT2 calculations could only be carried out to the limited size of 9 atoms as they become prohibitively more expensive, and at larger cluster size single reference MBPT2 will fail due to the closing 6*s*-6*p* gap. The CCSD(T) results are undoubtedly the most accurate, however, the BSSE correction (discussed later) becomes a much larger problem here compared to DFT. CCSD(T) calculations were only feasible up to a size of 7 atoms, where we have the first marked difference between the LJ and the Hartke isomer. We note that all Hartke structures have been reoptimized at the current level of theory. In most cases the resulting structure is still recognizably the structure as described in Ref. 19, however, for $N=8$ we see considerable structural changes.

TABLE II. LJ isomers, optimized with DFT (LDA, PW91), MBPT2, and CCSD(T) methods. The binding energy (BE) and binding energy per atom (BE/N) are in eV, the shortest bond length in the cluster ($r_{\min}$) is given in Å.

N	Symmetry	BE	BE/N	$r_{\min}$
		DFT (LDA)		
2	$D_{\infty h}$	−0.21	−0.107	3.107
3	D_{3h}	−0.61	−0.205	3.100
4	T_d	−1.20	−0.301	3.102
5	D_{3h}	−1.71	−0.341	3.109
6	O_h	−2.19	−0.365	3.173
7	D_{5h}	−2.86	−0.408	3.162
8	D_{2d}	−3.42	−0.427	3.109
9	C_{2v}	−4.12	−0.457	3.094
10	C_{3v}	−4.79	−0.479	3.100
11	C_{2v}	−5.45	−0.495	3.055
12	C_{5v}	−6.15	−0.512	3.046
13	I_h	−6.93	−0.533	3.111
14	C_{3v}	−7.55	−0.540	3.097
		DFT (PW91)		
2	$D_{\infty h}$	−0.06	−0.031	3.508
3	D_{3h}	−0.18	−0.058	3.491
4	T_d	−0.35	−0.087	3.457
5	D_{3h}	−0.50	−0.101	3.438
6	O_h	−0.64	−0.107	3.505
7	D_{5h}	−0.86	−0.122	3.479
8	D_{2d}	−0.99	−0.123	3.470
9	C_{2v}	−1.23	−0.137	3.435
10	C_{3v}	−1.44	−0.144	3.406
11	C_{2v}	−1.64	−0.149	3.395
12	C_{5v}	−1.87	−0.156	3.373
13	I_h	−2.14	−0.165	3.392
14	C_{3v}	−2.32	−0.166	3.385
		MBPT2		
2	$D_{\infty h}$	−0.03	−0.016	3.784
3	D_{3h}	−0.11	−0.036	3.684
4	T_d	−0.25	−0.063	3.556
5	D_{3h}	−0.40	−0.081	3.479
6	O_h	−0.55	−0.091	3.552
7	D_{5h}	−0.78	−0.112	3.487
8	C_{2v}	−0.93	−0.116	3.386
9	C_{2v}	−1.22	−0.136	3.361
		CCSD(T)		
2	$D_{\infty h}$	−0.01	−0.007	4.058
3	D_{3h}	−0.04	−0.014	3.996
4	T_d	−0.09	−0.024	3.919
5	D_{3h}	−0.15	−0.029	3.894
6	O_h	−0.20	−0.033	3.900
7	D_{5h}	−0.28	−0.040	3.762

TABLE III. Hartke (Ref. 19) isomers, optimized with DFT (LDA, PW91), MBPT2, and CCSD(T) methods. The binding energy (BE) and binding energy per atom (BE/N) are in eV, the shortest bond length in the cluster ($r_{\min}$) is given in Å.

N	Symmetry	BE	BE/N	$r_{\min}$
		DFT (LDA)		
7	D_{3d}	−2.50	−0.358	3.050
8	C_{2v}	−3.26	−0.407	3.152
9	D_{3h}	−4.12	−0.458	3.094
10	C_{3v}	−4.74	−0.474	3.086
11	D_{3h}	−5.33	−0.484	3.080
12	C_1	−6.00	−0.500	3.060
13	C_1	−6.76	−0.520	3.046
14	C_1	−7.35	−0.525	3.021
		DFT (PW91)		
7	D_{3d}	−0.73	−0.104	3.384
8	C_{2v}	−0.98	−0.122	3.468
9	D_{3h}	−1.17	−0.130	3.452
10	C_{3v}	−1.36	−0.136	3.437
11	D_{3h}	−1.54	−0.140	3.415
12	C_1	−1.75	−0.145	3.346
13	C_1	−1.94	−0.149	3.313
14	C_1	−2.15	−0.153	3.352
		MBPT2		
7	D_{3d}	−0.57	−0.082	3.485
8	C_{2v}	−0.91	−0.114	3.414
9	D_{3h}	−1.10	−0.122	3.423
		CCSD(T)		
7	D_{3d}	−0.20	−0.029	3.835

The CCSD(T) optimizations for Hg_7 were performed under symmetry constraints, i.e., both isomers (LJ and Hartke) have only two internal coordinates to be optimized. These structures are compared in Fig. 3, with the variable bonds and angles labeled, that is the two bond lengths R_1 and R_2 or, alternatively, one bond length R_1 and an angle A_1. The CCSD(T) results for Hg_7 are consistent with the LDA, PW91, and MBPT2 calculations, with weaker bonding characteristic of the CCSD(T) calculations, that is the LJ (D_{5h}) isomer is more stable at every level of calculation. The CCSD(T) calculation finds the LJ isomer to be 0.078 eV more stable compared to the Hartke isomer, which is larger than the dissociation energy of Hg_2 (0.050 eV). Moreover both the DFT and MBPT2 calculations found that the Hartke structure is a higher-order saddle point, with two and three imaginary vibrational frequencies, respectively.

In Fig. 2 are shown three isomers for $N=8$, where 8a is the LDA optimized LJ isomer, 8b is the isomer presented by Hartke *et al.*, and 8c is the MBPT2 optimized LJ isomer. While the underlying construction of 8a and 8c is quite similar, we present here both structures to indicate the range within which these structures vary when optimized by different *ab initio* methods. For $N=8$ both structures are realistic

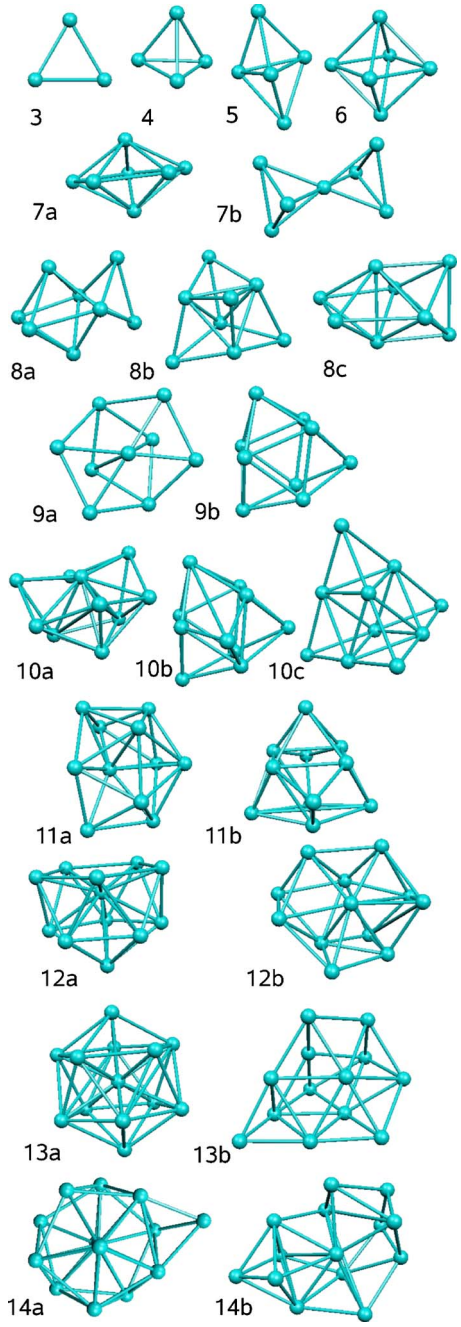

FIG. 2. (Color online) Structures of small Hg clusters. The isomers labeled "a" are referred to as the LJ isomers in the text, the isomers labeled "b" are those reoptimized from Ref. 19. In some cases there is a third low energy isomer shown as described in the text.

possibilities with quite highly symmetric structures. With the inclusion of a zero-point vibrational energy correction, the difference between the isomers becomes negligible.

It has recently been proposed[47] that at certain sizes perfect tetrahedra may be formed ($N=4,10,20,35,56,\ldots$), and that these tetrahedra may be in some cases lower in energy than the corresponding LJ structures. The case of $N=4$ is a trivial case. However, it is of interest to examine the case of $N=10$ for mercury. The structure was optimized using PW91 and the stability examined by a frequency analysis. The starting coordinates were taken from the supplementary data of Ref. 47. The resulting structure is compared with other isomers for $N=10$ in Table IV. The zero point vibrational energy (ZPVE) correction is reasonably large relative to the total binding energy, however, it has no effect on the relative energies of the different isomers. While the tetrahedral isomer 10c is a local minimum determined by a frequency analysis, it is also clearly less stable than the LJ isomer 10a. It is, however, more stable than the Hartke structure 10b. In the case of cadmium,[47] it was postulated that the increased stability of the tetrahedral isomers relative to the Lennard-Jones isomers could be related to the strong anisotropic ratio (c/a) of the bulk hcp lattice, which is the largest of all metals. However, the rhombohedral lattice of mercury can be considered to be even more anisotropic. This difference could be explained from the earlier onset of metallicity in Cd clusters than in Hg ones, which implies that the physics of small Cd clusters may be closer to that of the bulk than is observed for Hg.

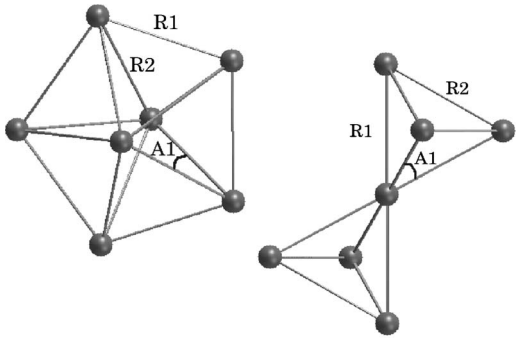

FIG. 3. The structures of the two Hg_7 isomers. The D_{5h} (LJ) isomer (left) is described by $R_1=3.938$ and $R_2=3.833$, $A_1=58.159$. The D_{3d} isomer (right) has $R_1=3.835$ and $R_2=4.096$, $A_1=64.556$, according to the CCSD(T) optimization. Bond lengths R_1 and R_2 are in Å, angles A_1 in deg.

The vibrational frequencies were calculated for each isomer in both DFT (LDA, PW91) and MBPT2, after optimization. All the LJ isomers were found to be minima on the potential energy surface, with no imaginary frequencies of vibration, except for some of the Hartke isomers. The $N=7$ case has already been mentioned, and for $N=12$ and 13 the PW91 calculation found the Hartke isomers to be transition states as well. The others are all local minima. To summarize, the isomers found by Hartke *et al.* are compared to the standard LJ isomers in Fig. 4 which highlights the energy difference between the two isomers. In all cases, the energy of the LJ isomer is lower, however, there are a few cases (notably $N=8$ and 9) where the energy differences become quite close.

The energies of the small LJ clusters are plotted in Fig. 5. There is at least a qualitative agreement between the various methods used [DFT, MBPT2, and CCSD(T)]. The LDA energies are consistently overbinding as expected, and therefore show a much quicker convergence towards the bulk cohesive energy. MBPT2 seems to perform slightly better than DFT, but, as for the dimer where the dissociation energy is known to reasonable accuracy, is still overbinding.[41] The CCSD(T) values are the best as expected. It is apparent that

TABLE IV. A comparison of the PW91 structures for Hg_{10}. The binding energy (BE) and the binding energy with zero-point vibrational correction (BE+ZPVE) included are in eV, and the shortest bond length (r_{min}) is in Å. The isomers are labeled a–c as in Fig. 2.

Isomer	BE	BE+ZPVE	r_{min}
Tetrahedral (10c)	−1.366	−1.325	3.4066
Lennard-Jones (10a)	−1.437	−1.396	3.4064
D_{3d} (from Ref. 19) (10b)	−1.358	−1.317	3.4369

the binding in these clusters is much weaker, and therefore a much slower progression towards the bulk is observed for the small sizes calculated. However, due to the limited size of the basis set available to our CCSD(T) calculations, the BSSE becomes non-negligible. We therefore obtained an estimate for the BSSE at the CCSD(T) level of theory for clusters between $N=2-6$ by calculating the sum of the BSSE error in each pair interaction derived from the Hg_2 potential curve. The subsequent binding energies are given in Table V together with the BSSE correction. Another slightly smaller contribution to the binding energy is the spin-orbit (SO) interaction, which has been approximated according to the equation in Ref. 36 taken from Ref. 48. Then the total energy (energy+BSSE+SO) was optimized locally to give the best approximation of the actual binding of each cluster.

It is evident that the BSSE correction worsens the agreement with experiment for the dimer, making the bond lengths considerably too long. However, it may be taken as an upper bound on the error induced by this basis set. This does mean that the errors in both bond lengths and energies are greater than desired. Moreover, the BSSE increases with decreasing distance of the atoms,[36,41] that is the BSSE becomes more notable if one moves towards the bulk. However, larger coupled cluster calculations were computationally not feasible and the BSSE correction does not change the relative ordering of the different isomers. Nevertheless, it is reassuring that despite the large energy differences produced by the different methods, the optimized structures are consistently

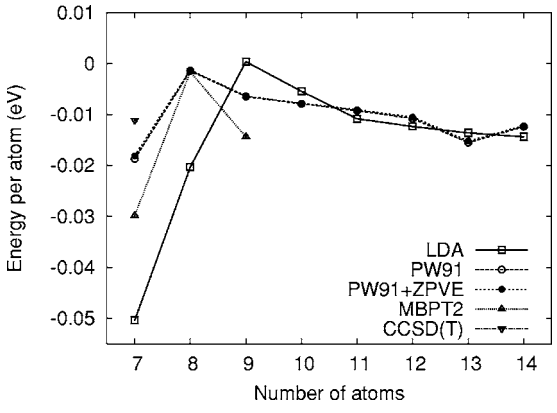

FIG. 4. Binding energy difference between LJ clusters and Hartke isomers in eV per atom. A zero-point vibrational energy (ZPVE) correction is added to the PW91 energies for comparison, calculated in the harmonic approximation as $\Sigma_i \hbar\omega_i/2$. A negative energy difference means that LJ is the most stable arrangement.

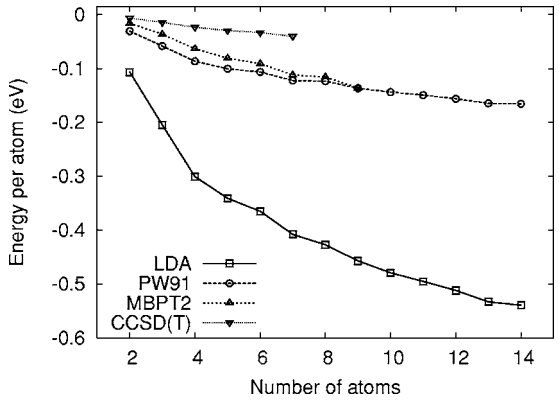

FIG. 5. Binding energy of LJ clusters per atom.

reproduced though with a bond length scaled according to the method used. The LDA clusters all have close to a constant (shortest) bond length, ranging between 3.0 and 3.2 Å, while the CCSD(T) bond lengths range from 3.8 to 4.1 Å for the clusters with $N \leq 7$. The PW91 and MBPT2 calculations show a similar trend, ranging between 3.3 and 3.8 Å. The minimum bond length decreases with cluster size N, as expected as the binding energy per atom is also increased. This decrease is more pronounced for MBPT2 than for PW91.

C. Two-body forces and the bulk

The experimentally determined structure of solid mercury has been extensively studied and is well known. Mercury freezes at 233 K, and forms a rhombohedral lattice with $a=3.005$ Å and $\alpha=70.53°$. Below 79 K it transforms into β-Hg, which has a tetragonal structure. Calculations using DFT, however, produce a surprising variety of numbers for the rhombohedral phase. The cohesive energies E_{coh} for bulk mercury at the experimental solid-state structure range from −0.17 eV (unbound, B3LYP) to 1.00 eV (LDA) through 0.01 eV (BP86), 0.14 eV (PBE), and 0.18 eV (PW91). The experimental cohesive energy is 0.67 eV.[6] Of these, LDA is the best performing functional for the solid as it is derived from the electron gas model and also gives reasonable lattice constants ($a=3.00$ Å and $\alpha=71.3°$). With all the other functionals tested the angle goes to $\alpha \approx 60°$. At the B3LYP level of theory the atoms are not bound in the solid. Although in a global optimization LDA gets the rhombohedral angle correct, this appears to be due primarily to the overbinding of

TABLE V. The effect of the basis set superposition error and spin-orbit interaction to the binding energy for cluster sizes $N=2-6$, per atom. r_{min} is the shortest bond length in Å, obtained at the [CCSD(T)+BSSE+SO] level of theory. All energies are in eV.

N	r_{min}	BE/N	BSSE/N	SO/N	BE(+BSSE+SO)/N
2	4.352	−0.011	0.008	−0.001	−0.004
3	4.329	−0.037	0.025	−0.002	−0.014
4	4.289	−0.076	0.056	−0.005	−0.025
5	4.173	−0.127	0.088	−0.008	−0.047
6	4.158	−0.176	0.123	−0.011	−0.065

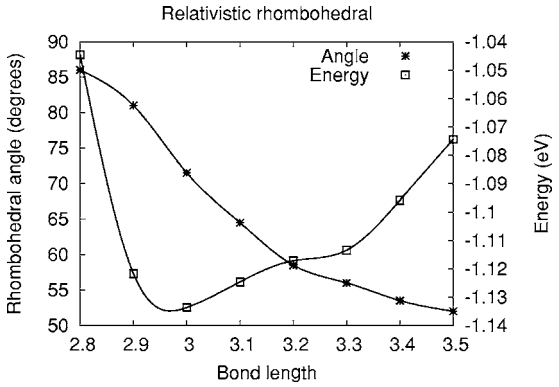

FIG. 6. The dependence of the rhombohedral angle on nearest neighbor distance, as calculated with LDA. The corresponding binding energy is also shown.

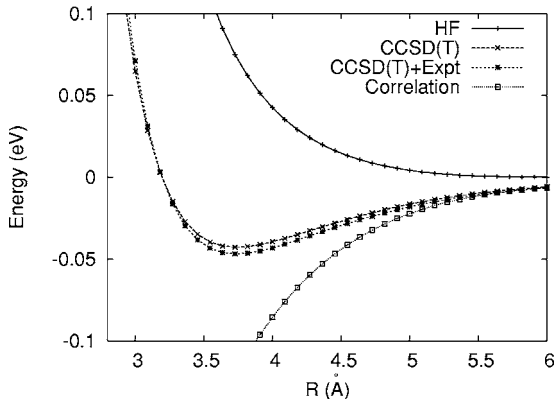

FIG. 7. The HF and correlation description of Hg_2.

LDA, as if the a is fixed at a higher value the angle will decrease towards 60°. This is shown in Fig. 6. Already at a =3.30 Å, the optimized angle with LDA becomes 60°. On the other hand, the PW91 functional gives larger angles at short bond lengths. When the bond length is reduced from the optimized value of a=3.54 Å to a=3.00 Å, α increases from 60° to 86°. Hence the rhombohedral angle α is very sensitive to the lattice constant a.

Equally disappointing is the performance of pure two-body potentials. It has been demonstrated[22] that not only three-body, but four-body and higher interaction terms are important for mercury clusters. For example, a recently determined empirical pair potential used for liquid/vapor phase simulations[49] yields for the solid at T=0 K a =3.04 Å, α=60.0°, E_{coh}=0.21 eV, and a zero-point energy of ω_0=72 cm^{-1} obtained from using the Einstein approximation (66 cm^{-1} derived from the Debye frequency).[51] In comparison, the simple Lennard-Jones potential[50] gives a =3.16 Å, α=60.0°, E_{coh}=0.63 eV, and ω_0=100 cm^{-1}. The most accurate potential curve as parametrized by Schwerdtfeger *et al.*[36] gives a=3.47 Å, α=60.0°, E_{coh}=0.42 eV, and ω_0=58 cm^{-1}. The difference to the experimental values is (in addition to minor corrections such as temperature) purely determined by three- and higher-body forces. It seems to be that all two-body potentials lead to an angle of α=60.0° and only vary in the cohesive energy and the lattice constant a. This angle of course reflects fcc packing, that is two-body potentials lead to closed packing and any distortion from fcc is due to higher than two-body effects. The particular stability of fcc packing is seen as a small dip in the energy curve of Fig. 6 at around a=3.30 Å.

Currently the best way to treat the solid-state for mercury is by a many-body electron correlation expansion derived from coupled-cluster theory for embedded clusters which is added to the solid state HF energy, as detailed by Paulus and co-workers.[25,52] They obtained a cohesive energy of 0.79 eV in good agreement with experiment. However, this method is computationally quite expensive. In a recent paper[25] we have shown that the many body expansion of the correlation energy

$$E_{cor} = \sum_{i<j} \Delta\epsilon_{ij} + \sum_{i<j<k} \Delta\epsilon_{ijk} + \cdots, \tag{4}$$

for Hg_6 converges much faster than the total energy, and that even at 3.0 Å the two-body part of the correlation energy contains 95% of the total energy. Therefore as it is precisely this part of the *ab initio* calculations that is most expensive, replacing the explicit calculation of correlation by a two-body correlation potential may allow us to optimize the structures of larger clusters more accurately than has been previously possible. We therefore attempted the parametrization of the two-body correlation potential obtained from the diatomic potential curve, and tested this approximation for the smallest cluster sizes and the solid state. For the solid this requires the calculation of the bulk HF energy and the subsequent addition of a simple two-body correlation energy term calculated over all pairs in the lattice.[51] This approach is not only computationally cheap, but is conceptually simple and may in principle be applied to all size ranges between the atom and the bulk.

For the smallest mercury clusters the HF potential was calculated using the large uncontracted basis set used for the dimer potential, with the addition of g and h functions. Here the BSSE at the HF level of theory becomes negligible. The sum of HF plus the parametrized two-body correction was then taken as the total energy of the cluster, and the structure was optimized with respect to this energy by varying the bond lengths. The initial coordinates were taken from the MBPT2 optimized structures described in Sec. III B.

In Fig. 7 the Hartree-Fock curves for the dimer are shown, calculated with our large uncontracted basis set. This is compared to the best potential curve for Hg_2, which is the CCSD(T) curve of Ref. 36 including spin-orbit effects and scaled to fit the experimental bond length and energy (3.69 Å, 400 cm^{-1}=0.0018 a.u.=0.05 eV). The correlation energy curve is simply the difference between the scaled CCSD(T) [CCSD(T)+expt.] curve and the HF potential. A simple function was fitted to the correlation energy curve which for convenience took the same form as that used for the CCSD(T) Hg_2 potential in Ref. 36. This is of the form

$$\Delta\epsilon_{ij} = \sum_{n=3}^{9} a_{2n} (r_{ij})^{-2n} \tag{5}$$

for a potential depending on the distance between two atoms r_{ij}. The coefficients a_{2n} are given in Table VI.

TABLE VI. The coefficients a_{2n} of Eq. (5) used for the correlation potential ($\Delta\epsilon$ in eV and r in a.u.).

a_{2n}	
a_6	4.5540579128E+01
a_8	−8.9370767041E+02
a_{10}	6.0974939151E+03
a_{12}	−2.1744291269E+04
a_{14}	4.3408446572E+04
a_{16}	−4.5875022175E+04
a_{18}	1.9971335911E+04

Table VII shows the total binding energy and the optimized bond lengths for clusters up to $N=8$. The agreement with the CCSD(T) structures of Ref. 53 is very good, as shown in Table VII. A final comparison of the energies and bond lengths of mercury clusters ($N=2-6$) obtained with different methods is given in Table VIII. Moving now to the solid state we obtain at the experimental lattice parameters $E_{\mathrm{HF}}=0.508$ eV, $E_{\mathrm{corr}}=-1.384$ eV, which gives for the total cohesive energy $E_{\mathrm{HF+corr}}=-0.876$ eV ($E_{\mathrm{coh}}=0.876$ eV). The discrepancy to the experimental value comes most likely from the HF part which is not repulsive enough due to basis set deficiencies and corresponding BSSE, plus higher than two-body effects in the correlation correction. Therefore we performed a counterpoise correction for the HF energy of the solid, where the basis functions of the 12 nearest neighbors were included in the atomic energy calculation. This results in a revision of the HF binding energy from 0.508 to 0.984 eV, and a total $E_{\mathrm{HF+corr}}=-0.399$ eV. This is a 54% decrease in the cohesive energy due to the BSSE. Larger basis sets could not be used due to convergence difficulties in the SCF procedure. An optimization of the lattice structure using the BSSE-corrected HF energy and the two-body correlation energy finds a minimum at lattice parameters 2.97 Å and $\alpha=68.5°$. The binding energy here is then $E_{\mathrm{coh}}=0.419$ eV, or 63% of the experimental value. However, we can expect this error to be considerably less for finite systems where we are able to use much better basis sets for the HF calculation, thereby reducing the error inherent in the BSSE correction.

TABLE VII. The HF+two-body correlation potential optimized clusters $N=2-6$, based on the global minimum LJ geometries. The CCSD(T) results are those of Ref. 53. For Hg_5 the bond length given is that of the axial-equatorial bond of the trigonal bipyramid [which are more numerous (6 pairs) than the longer axial-axial (1) or shorter equatorial-equatorial (3) bonds]. For Hg_6 and above the shortest bond is given.

	HF+correlation		CCSD(T) from Ref. 53	
N	r(Å)	BE (eV)	r(Å)	BE (eV)
2	3.762	−0.047	3.750	−0.046
3	3.542	−0.171	3.514	−0.183
4	3.359	−0.446	3.350	−0.472
5	3.438	−0.625	3.440	−0.695
6	3.501	−0.768	3.519	−0.792
7	3.452	−1.095		
8	3.487	−0.710	3.649[a]	−0.624[a]

[a]The CCSD(T) calculation for Hg_8 assumed a cubic structure.

TABLE VIII. Binding energies (BE) in eV and bond lengths (r) in Å, of mercury clusters ($N=2-6$) obtained with different methods. The CC′ results are the CCSD(T) results of this paper (without BSSE correction), the Dolg results are the CCSD(T) results of Ref. 53, the HFC results are the Hartree-Fock+two-body correlation results, and the $2+3n$ results are the simulated annealing results of Ref. 22.

	r				BE			
N	CC′	Dolg	HFC	$2+3n$	CC′	Dolg	HFC	$2+3n$
2	4.057	3.75	3.762	3.690	−0.022	−0.046	−0.046	−0.045
3	3.996	3.51	3.542	3.612	−0.111	−0.183	−0.171	−0.173
4	3.918	3.35	3.359	3.398	−0.412	−0.472	−0.446	−0.403
5	3.894	3.44	3.438	3.361	−0.635	−0.695	−0.626	−0.628
6	3.899	3.52	3.501	3.327	−1.056	−0.792	−0.767	−0.908

Another consideration is related to the pseudopotential approximation used for mercury (for both the cluster and solid calculations) which will introduce a small error in the repulsive region of the potential at small distances such as 3 Å, which is due to the neglect of innercore polarization and core-core repulsion effects. Nevertheless, this is a better result than what we have obtained with any density functional yet.

D. Polarizabilities

Polarizabilities are sensitive to structural changes and therefore useful to distinguish experimentally between different isomers of the same cluster size. In the following, the large and small basis sets are those used for the dimer potentials and the cluster optimizations, respectively. Small+spf refers to the basis set that we have used for all cluster polarizability calculations. The PW91 values for the atom are 15.51 a.u. (small), 34.61 a.u. (large), and 32.99 a.u. (small+spf). The experimental atomic polarizability of Hg is 33.92 a.u., taken from Goebel and Hohm.[54] This clearly shows the importance of diffuse and polarization functions.

Table IX compares the polarizability of each of the Hartke isomers with the corresponding LJ isomer. Clearly the average polarizability of the Hartke structures is higher, due to the lower symmetry and less compact arrangement. The difference is consistently about 1 a.u. per atom, with the exceptions of $N=10$, where the isomers have almost exactly equal polarizabilities per atom, and $N=13$, where the difference is almost 2.5 a.u. per atom. The first case can be understood as the Hartke structure for $N=10$ is quite far from compact compared to the LJ structure. Conversely the maximum difference seen for $N=13$ is due to the particularly high symmetry of the icosahedral LJ cluster, which results in a lower than otherwise expected polarizability. However, even

TABLE IX. Comparison of the PW91 polarizability for different Hg cluster isomers. The polarizability units are a.u.

	Isotropic polarizability		Anisotropic polarizability	
N	LJ isomers	Hartke isomers	LJ isomers	Hartke isomers
7	272.5	281.0	98.4	82.2
8	308.3	317.9	77.7	1.5
9	356.7	369.4	114.1	63.3
10	396.5	396.1	106.6	22.0
11	435.4	444.6	74.9	114.9
12	470.6	480.7	44.5	92.9
13	502.3	532.1	0.0	133.9
14	553.8	568.5	104.8	163.8

this difference is still only approximately 30 a.u., i.e., about 7% of the total polarizability value for $N=13$, and it will be difficult experimentally to distinguish between the different structures. However, less compact structures show large anisotropies which are also listed in Table IX. In particular we note the large difference in the polarizability anisotropy of the different isomers for $N=13$, as expected, but also for $N=8$, where the non-LJ isomer is more symmetric according to this measure than the LJ isomer.

In Fig. 8 are plotted the polarizability per atom of all clusters $N=1-24$, where the structures are the PW91 optimized geometries obtained from the LJ structures. Clear magic numbers are seen at $N=6,8,13,19$, and 23. These correspond to the most symmetric structures, the $N=6$ octahedron, the $N=8$ D_{2d} structure (based on the octahedron), and the icosahedral structures for $N=13,19$, and 23. This is in precise agreement with the magic numbers found previously by Moyano *et al.*.[22] These numbers are even more pronounced in the plot of the change in polarizability from $N\rightarrow N+1$ also shown in Fig. 8. However, we notice a change in the magic numbers observed when we plot the polarizability anisotropy. Here we see that $\beta(N)$ is zero for $N=1,4,6$, and 13. For the 19 and 23 atom clusters, where a sharp minimum was observed in the plot of the change in polarizability from $N\rightarrow N+1$, we observe a maximum in the polarizability anisotropy. Thus the anisotropy is more sensitive to deformation along one axis such as in the prolate 19-atom cluster or the oblate 23-atom cluster, while the isotropic polarizability remains small.

In contrast to the Zn_N cluster polarizabilities in Ref. 27, we find a smooth convergence to a limiting value in our plot of polarizability per atom, with deviations due only to the magic numbers. However, these become smaller with increasing cluster size. Papadopoulos *et al.* [27] consider sharp changes in the Zn_N cluster polarizabilities as an indication of changes in the strength of bonding, and thus a transition from van der Waals to covalent type bonding. In our case we do not see a clear transition and the change is rather smooth.

In contrast to what is expected for metal clusters, the per atom polarizability here increases with size. This is clearly explained as the interaction of two closed-shell atoms produces a diffuse antibonding orbital and thus increases the polarizability. The classical limit of a conducting sphere has

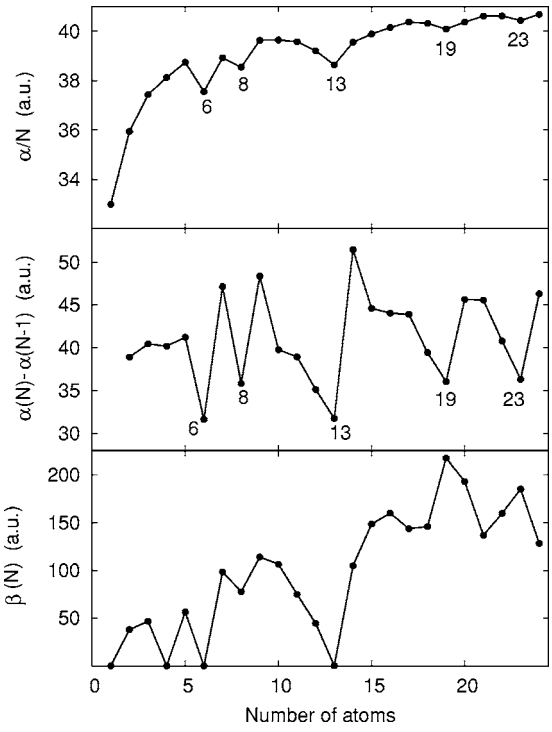

FIG. 8. Top: The isotropic polarizabilities (per atom) of LJ clusters, calculated with PW91. Center: The change in polarizability as $\alpha(N)-\alpha(N-1)$. The "magic numbers" corresponding to highly symmetric structures are marked. Bottom: The polarizability anisotropy $\beta(N)$. Here the anisotropy goes to zero for the cases of highest symmetry $N=1,4,6,13$.

been frequently used to justify the parametrization $\alpha=R_{eff}^3$, where $R_{\text{eff}}=R_n+\delta$ and R_n is the core radius (the Wigner-Seitz radius in the case of the bulk). Then δ represents the electron spill out from the ionic boundary. Within this model the per atom polarizability for metal clusters must decrease as a function of N from the atomic value[54] (33.92 a.u.) to the bulk limit[55] (18.61 a.u.; $r_s=1.40$ Å at 78 K). It can be imagined that the per atom polarizability will therefore increase while the covalency of the cluster is increasing at small sizes, as is seen here, start to decrease when the transition from covalent to metallic bonding takes place, and only then (after the experimentally suggested value of around 400 atoms, for example) begin to descend towards the bulk limit.

IV. CONCLUSIONS

In analogy with the noble gas clusters, the most stable isomers for small sizes of mercury clusters are the symmetric, LJ type at all levels of theory, that is DFT, MBPT2, and CCSD(T). The best description of their structure and energy is obtained using coupled cluster methods or alternatively our HF plus two-body correlation approach, which should also work for larger systems. Improved calculations will only be convincing with the use of a high-level correlation method (e.g., multireference configuration interaction) with a basis set larger than here to minimize the BSSE, which is currently prohibitive. In the case of DFT the choice of functional plays an important role; PW91 seems to describe the

bonding of small systems best, albeit not that accurately. Such an *ad hoc* choice of functional is a very unsatisfactory situation and has to be addressed in future DFT development. The use of a two-body potential to correct Hartree-Fock for correlation looks very promising. Although our results are preliminary, they do cover a wide range of structures. Both for the clusters and for the bulk, the two-body correction seems to be very accurate with reference to the best data that we have to compare with. This simple ansatz of a two-body correlation potential can be expected to have wide applicability for mercury clusters and for the simulation of solid to liquid phase transitions.

The polarizability of the calculated mercury clusters increases over the range studied, with no transition from van der Waals type to covalent bonding visible. This is in agreement with the accepted value (around 400 atoms) for the transition in mercury according to experiment, but is in contrast to some recent results for zinc.[27]

ACKNOWLEDGMENTS

N.G. is grateful for support from the New Zealand Tertiary Education Commission. P.S. is grateful to Tilo Söhnel for useful discussions. This work was supported by a Marsden grant administered by the Royal Society of New Zealand.

[1] *Theory of Atomic and Molecular Clusters*, edited by J. Jellinek, Springer Series in Cluster Physics (Springer, Heidelberg, 1999).
[2] *Clusters of Atoms and Molecules*, edited by H. Haberland, Vols. 52 and 56 of Springer Series of Chemical Physics (Springer, Heidelberg, 1994).
[3] *Large Clusters of Atoms and Molecules*, edited by T. P. Martin, NATO ASI Series in Applied Sciences (Plenum, New York, 1995).
[4] W. A. de Heer, Rev. Mod. Phys. **65**, 611 (1993).
[5] R. D. van Zee, S. C. Blankespoor, and T. S. Zwier, J. Chem. Phys. **88**, 4650 (1988).
[6] *The CRC Handbook of Chemistry and Physics*, edited by D. R. Lide (CRC Press, New York, 2002).
[7] C. Bréchignac, M. Broyer, P. Cahuzac, G. Delacretaz, P. Labastie, J. P. Wolf, and L. Wöste, Phys. Rev. Lett. **60**, 275 (1988).
[8] D. J. Wales, J. P. K. Doye, A. Dullweber, M. P. Hodges, F. Y. Naumkin, F. Calvo, J. Hernádez-Rojas, and T. F. Middleton, The Cambridge Cluster Database, URL http://www-wales.ch.cam.ac.uk/CCD.html
[9] K. Rademann, O. Dimopoulou-Rademann, M. Schlauf, U. Even, and F. Hensel, Phys. Rev. Lett. **69**, 3208 (1992).
[10] B. Kaiser and K. Rademann, Phys. Rev. Lett. **69**, 3204 (1992).
[11] P. P. Singh and K. S. Dy, Z. Phys. D: At., Mol. Clusters **17**, 309 (1990).
[12] M. E. Garcia, G. M. Pastor, and K. H. Bennemann, Phys. Rev. Lett. **67**, 1142 (1991).
[13] H. Ito, T. Sakurai, T. Matsuo, T. Ichihara, and I. Katakuse, Phys. Rev. B **48**, 4741 (1993).
[14] R. Busani, M. Folkers, and O. Cheshnovsky, Phys. Rev. Lett. **81**, 3836 (1998).
[15] H.-J. Flad, F. Schautz, Yixuan Wang, M. Dolg, and A. Savin, Eur. Phys. J. D **6**, 243 (1999).
[16] Y. Wang, H.-J. Flad, and M. Dolg, Int. J. Mass. Spectrom. **201**, 197 (2000).
[17] Y. Wang, H.-J. Flad, and M. Dolg, Phys. Rev. B **61**, 2362 (2000).
[18] M. Dolg and H.-J. Flad, Mol. Phys. **91**, 815 (1997).
[19] B. Hartke, H.-J. Flad, and M. Dolg, Phys. Chem. Chem. Phys. **3**, 5121 (2001).
[20] B. Hartke, Angew. Chem., Int. Ed. **41**, 1468 (2002).
[21] J. P. K. Doye, D. J. Wales, and R. S. Berry, J. Chem. Phys. **103**, 4234 (1995).
[22] G. E. Moyano, R. Wesendrup, T. Söhnel, and P. Schwerdtfeger, Phys. Rev. Lett. **89**, 103401 (2002).
[23] K. Rosciszewski, K. Doll, B. Paulus, P. Fulde, and H. Stoll, Phys. Rev. B **57**, 14 667 (1998).
[24] H. Stoll, B. Paulus, and P. Fulde, J. Chem. Phys. **123**, 144108 (2005).
[25] B. Paulus, K. Rościszewski, N. Gaston, P. Schwerdtfeger, and H. Stoll, Phys. Rev. B **70**, 165106 (2004).
[26] P. Schwerdtfeger, N. Gaston, R. P. Krawczyk, R. Tonner, and G. E. Moyano, Phys. Rev. B **73**, 064112 (2006).
[27] M. G. Papadopoulos, H. Reis, A. Avramopoulos, S. Erko, and L. Amirouche, J. Phys. Chem. B **109**, 18822 (2005).
[28] G. Tikhonov, V. Kasperovich, K. Wong, and V. V. Kresin, Phys. Rev. A **64**, 063202 (2001).
[29] M. B. Knickelbein, J. Chem. Phys. **115**, 5957 (2001).
[30] M. B. Knickelbein, J. Chem. Phys. **118**, 6230 (2003).
[31] M. B. Knickelbein, J. Chem. Phys. **120**, 10450 (2004).
[32] M. J. Frisch *et al.*, *Gaussian* 03, Revision B.03 (Gaussian, Pittsburgh, PA, 2003).
[33] H.-J. Werner, P. J. Knowles, R. Lindh, M. Schütz, P. Celani, T. Korona, F. R. Manby, G. Rauhut, R. D. Amos, A. Bernhardsson, A. Berning, D. L. Cooper, M. J. O. Deegan, A. J. Dobbyn, F. Eckert, C. Hampel, G. Hetzer, A. W. Lloyd, S. J. McNicholas, W. Meyer, M. E. Mura, A. Nicklass, P. Palmieri, R. Pitzer, U. Schumann, H. Stoll, A. J. Stone, R. Tarroni, and T. Thorsteinsson, MOLPRO, version 2002.6, a package of *ab initio* programs, http://www.molpro.net/, Birmingham, UK, 2003.
[34] D. Andrae, U. Haeussermann, M. Dolg, H. Stoll, and H. Preuss, Theor. Chim. Acta **77**, 123 (1990).
[35] S. F. Boys and F. Bernardi, Mol. Phys. **19**, 553 (1970).
[36] P. Schwerdtfeger, R. Wesendrup, G. E. Moyano, A. J. Sadlej, J. Greif, and F. Hensel, J. Chem. Phys. **115**, 16 (2001).
[37] V. R. Saunders, R. Dovesi, C. Roetti, R. Orlando, C. M. Zicovich-Wilson, N. M. Harrison, K. Doll, B. Civalleri, I. J. Bush, Ph. D'Arco, and M. Llunell, CRYSTAL03, www.crystal.unito.it, Turin, 2003.
[38] B. Paulus (private communication).
[39] A. D. Buckingham, Adv. Chem. Phys. **12**, 107 (1967).
[40] M. Yu and M. Dolg, Chem. Phys. Lett. **273**, 329 (1997).
[41] P. Schwerdtfeger, J. Li, and P. Pyykkö, Theor. Chim. Acta **87**, 313 (1994).

[42] V. Boutou, A. R. Allouche, F. Spiegelmann, J. Chevaleyre, and M. Aubert Frécon, Eur. Phys. J. D **2**, 63 (1998).
[43] M. A. Czajkowski and J. Koperski, Spectrochim. Acta, Part A **55**, 2221 (1999).
[44] J. Koperski, J. B. Atkinson, and L. Krause, Chem. Phys. Lett. **219**, 161 (1994).
[45] A. R. Allouche, M. Aubert-Frécon, G. Nicolas, and F. Spiegelmann, Chem. Phys. **200**, 63 (1995).
[46] Y. Wang, H.-J. Flad, and M. Dolg, Phys. Rev. B **61**, 2362 (2000).
[47] M. P. Johansson and P. Pyykkö, Phys. Chem. Chem. Phys. **6**, 2907 (2004).
[48] M. Dolg and H.-J. Flad, J. Chem. Phys. **100**, 6147 (1996).
[49] J.-M. Bomont and J.-L. Bretonnet, J. Chem. Phys. **124**, 054504 (2006).
[50] J. O. Hirschfelder, C. F. Curtiss, and R. B. Bird, *The Molecular Theory of Gases and Liquids* (Wiley, New York, 1964).
[51] P. Schwerdtfeger, Program SAMBA: A solid state approach using a many body ansatz, Massey University, Auckland, 2006.
[52] B. Paulus, Phys. Rep. **428**, 1 (2006).
[53] M. Dolg and H.-J. Flad, Mol. Phys. **91**, 815 (1997).
[54] D. Goebel and U. Hohm, J. Phys. Chem. **100**, 7710 (1996).
[55] N. W. Ashcroft and N. D. Mermin, *Solid State Physics* (Brooks-Cole, Cornell University, 1976).